Soliton based Dynamic Nuclear Polarization: an unexpected Overhauser effect in cyclic polyacetylene at high field and room temperature

Z. Miao,[1] F. J. Scott,[2] J. van Tol,[2] C. R. Bowers,[1, 2] A. S. Veige,[1] F. Mentink-Vigier[2]*

[1]Department of Chemistry, University of Florida, Center for Catalysis, Gainesville, FL, USA

[2]National High Magnetic Field Laboratory, Florida State University, 1800 E. Paul Dirac Dr, 32310, Tallahassee, FL, USA

* Frederic Mentink-Vigier: fmentink@magnet.fsu.edu

ABSTRACT

Polyacetylene, a versatile material with an electrical conductivity that can span seven orders of magnitude, is the prototypical conductive polymer. In this letter, we report an unexpected and unprecedented Overhauser Effect that increases with temperature, observed under high magnetic field of 14.1 T, in both linear and cyclic polyacetylene. Significant NMR signal enhancements ranging from 24 to 45 are obtained. The heightened sensitivity enabled the characterization of chain defects at natural abundance. The absence of end methyl group carbon-13 signals provides proof of the closed-loop molecular structure of the cyclic polyacetylene. This efficiency of the soliton based Overhauser Effect DNP mechanism at high temperature and high field holds promise for applications and extension to other conductive polymer systems.

KEYWORDS EPR, cyclic polymer, conductive polymer, NMR, Magic Angle Spinning, MAS-DNP

In recent years, the research and utilization of conductive polymers has expanded significantly, with applications spanning from optoelectronics to material science.[1] Linear polyacetylene (linear PA), the simplest polyene and the most extensively studied organic conjugated polymer, was first synthesized using titanium-based catalysts by Natta in 1958.[2] A major breakthrough occurred when Shirakawa synthesized free standing films of linear PA, endowing PA materials both mechanical flexibility as a polymer film[3,4] and, after doping, conductivities comparable to metals.[5,6] When synthesized at -78 °C using Shirakawa's method, linear PA contains *cis* double bonds as a natural consequence of an insertion mechanism[2] but the more stable *trans-transoid* isomer with higher conductivities can be obtained via thermal isomerization.[3,7] In 2022, we reported the synthesis of cyclic polyacetylene (cyclic PA; Figure 2).[8–10] Unique to its topology, cyclic PA synthesized with catalyst **1**[11–15] (Scheme 1) exhibits an exclusively *trans-transoid* structure, even at -94 °C.[9]

Producing and characterizing such conductive polymer is a challenge because it is insoluble. For such materials, solid-state NMR provides unrivaled structural information at the atomic scale. However, conventional solid-state NMR is a notoriously insensitive technique which makes it challenging to detect chemical sites at low concentrations. The sensitivity of solid-state NMR can be increased by combining magic angle spinning (MAS) with Dynamic Nuclear Polarization (MAS-DNP). In this method the nuclear spins are hyperpolarized via high power irradiation of electron spin resonance transitions associated with paramagnetic centers.[16–21] With only a few notable exceptions,[22–24] MAS-DNP under magnetic fields is carried out with extrinsic paramagnetic species at low temperature where the electron and nuclear spin dynamics is more favorable.[25–27] DNP using intrinsic paramagnetic species is interesting as it directly probes the properties, spin interactions, and spin dynamics of the material itself.[28–30] In addition, DNP requires the sample to be transparent to □w irradiation. The skin depth in conductors is inversely proportional to the □w frequency, which limits the volume of sample that is effectively irradiated and can result in sample heating. Therefore, reports of MAS-DNP carried out with unpaired electrons at room temperature in organic materials at high fields are extremely rare, and to our knowledge, DNP in a conductive organic solid under high magnetic field (≥14.1 T) has not been previously reported. In this letter we report the unexpected strong ^{1}H MAS-DNP signal enhancements ranging between 20 and 50 in undoped linear and cyclic polyacetylene (*trans-transoid*),[31] hereafter referred to as linear PA and cyclic PA, at high field and room temperature. The nature and origin of these remarkable signal enhancements have been determined with the help

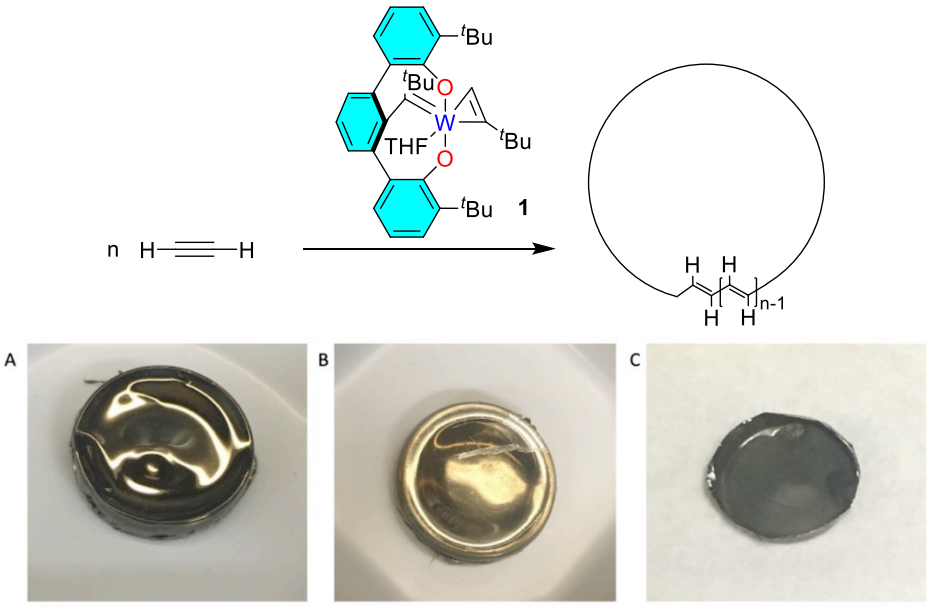

Scheme 1. Synthesis of cyclic polyacetylene with catalyst **1**. Panels A-C depicts various samples of cyclic polyacetylene that can be produced with catalyst **1**.

of EPR studies and numerical simulations based on the Overhauser and Solid Effect mechanisms. These large enhancements enabled us for the first time to analyze the topological and chemical defects in the novel cyclic conductive polymer.[31] The data quality suggests the method could be extended to other conductive polymers.[1,32]

Conductive polymers such as polyacetylene contain defects in the π-conjugation called solitons that bear isolated unpaired electrons.[32] Thus, linear and cyclic polyacetylene samples were initially characterized by EPR. The room temperature X-band EPR spectra (9.6 GHz / 0.3 T) presented in Fig. S1 of the Supporting Information (S.I.) exhibit a single, featureless resonance reflecting the high mobility of the conductive electrons which averages the local spin interactions, i.e., the g-tensor and hyperfine couplings. Indeed, the correlation time, τ_c, is much faster than the inverse of the largest hyperfine coupling, $\frac{1}{|A|_{\max}} \approx \frac{1}{18}$ MHz[33] with an upper bound of 10^{-13} s.[34] To obtain more information we conducted the variable temperature high-field EPR spectra experiments acquired at 8.4 T/240 GHz. At this field, the impact of the g-tensor anisotropy on the EPR spectra is more important, and the motional narrowing has a lower impact. The experimental results are shown in Figure 1. In both samples, the EPR broadens as the temperature is reduced from 220 K to 10 K. The EPR spectra of the linear PA exhibit additional features at lower temperatures. This observation aligns with the existing literature, suggesting the presence of two distinct spin populations in linear PA: one comprised of electron spins delocalized in the conduction band, and another trapped in localized defects.[32,34] As the temperature decreases, the delocalized electrons become trapped within the defects, leading to a reduction in motional narrowing. The soliton mobility in cyclic PA appears to follow the same trend. The EPR line exhibits some degrees of asymmetry as the temperature is lowered, also indicating reduced motional narrowing. However, at 10 K the EPR line of cyclic PA is twice as narrow as the linear PA line and presents fewer features. This suggests that the reduction in mobility within cyclic PA appears less pronounced compared to its linear counterpart. This is consistent with a lower density of chain defects in the cyclic PA sample and/or a soliton trapping potential that is shallower compared to that of the linear PA sample.[34,35]

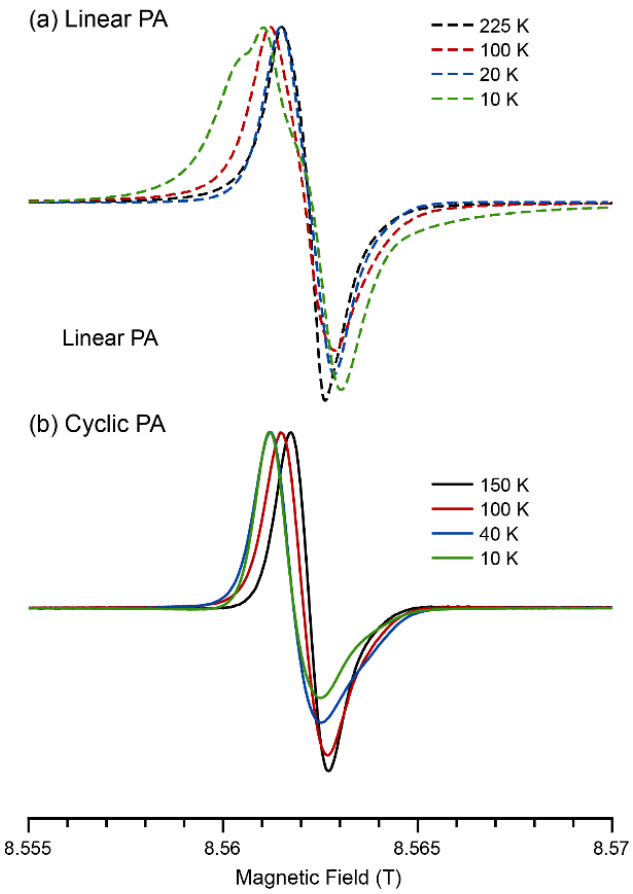

Figure 1 EPR spectra as a function of temperature of (a) linear PA and (b) cyclic PA collected between 225 K and 10 K at a μw frequency of 240 GHz.

MAS-DNP NMR experiments were performed on linear and cyclic PA samples at magnetic fields around 14.1 T or 600 MHz ^{1}H Larmor frequency. Figure 2 depicts the ^{1}H NMR signal enhancements plotted as a function of the static magnetic field for a fixed microwave frequency of 395.145 GHz. Both samples exhibit maximum enhancement of the ^{1}H nuclear spin polarization for microwave irradiation (μw) at the EPR resonance condition. Significant enhancements of 22 and 30 were obtained for linear PA and cyclic PA, respectively. In addition, a modest nuclear spin depolarization is observed at the lower field of 14.078 T. The enhancements in the vicinity of ~14.095 T have constant sign which is characteristic of the Overhauser Effect (OE) mechanism.[36–38] In addition, the maximum enhancement is obtained for a modest μw irradiation strength (~8 W at 100

K, see Fig. S2) while the depolarization at ~14.078 T (≡ 600 MHz lower Larmor Frequency) is due to the Solid-Effect (SE)[39,40] mechanism where irradiation of the double quantum electron-nucleus transition generates a polarization below thermal equilibrium.

Depicted in Figure 2(a), in cyclic PA the enhancement due to the OE is significantly larger than for the SE, as it reaches 30 while for the SE it is only ~0.6. For the linear PA sample, the OE enhancement is as high as 22 but only 0.7 for the SE condition. The observation of the OE relates to the presence of fluctuating isotropic hyperfine couplings, that can be attributed to the conduction electron.[36,41] Nevertheless, the identification of the SE DNP mechanism implies that the anisotropic hyperfine coupling is not entirely averaged at 100 K. This suggests that either the motional averaging resulting from electron spin delocalization is incomplete or that there are two distinct types of defect "sites". The former assertion aligns with experimental findings in linear polyacetylene,[34,42] the high field EPR measurements, and it is reasonable to extend this assumption to cyclic PA as well. Since the two electron spin populations have identical Larmor frequencies, the enhancement field profile was simulated by considering the coupling between n electron spins and N_1 nuclear spins on site #1 and N_2 nuclear spins on site #2. The corresponding rotating frame spin Hamiltonian is given by:

$$\begin{aligned}\hat{H}_0 = &\sum_{l=1}^{n}((g\beta B_0 - \Delta\omega)\hat{S}_{z,l} + \omega_1\hat{S}_{x,l} \\ &+ \sum_{k=1}^{N_1} A_{z,l,k}^{\mathrm{iso}}\hat{S}_{z,l}\hat{I}_{z,k} \\ &+ \sum_{k=1}^{N_2} +2A_{z,l,k}^{\mathrm{aniso}}\hat{S}_{z,l}\hat{I}_{z,k} \\ &+ A_{+,k}^{\mathrm{aniso}}\hat{S}_{z,l}\hat{I}_{+,l,k} \\ &+ A_{-,k}^{\mathrm{aniso}}\hat{S}_{z,l}\hat{I}_{-,l,k}\end{aligned} \qquad \text{Eq. (1)}$$

The first two terms relate to the Zeeman and ⍰w interactions, while the remaining terms represent the hyperfine couplings to the nuclei. Due to the fact that the two mechanisms are well separated in frequency, the problem can be reduced to a simple “two-spin” system where only the “average” hyperfine couplings are considered for each of the two populations:

$$\begin{aligned}\hat{H}_0 = &(g\beta B_0 - \Delta\omega)\hat{S}_z + \omega_1\hat{S}_x \\ &+ \hat{S}_z\big(\langle 2A_{z,k}^{\mathrm{iso}} + A_{z,k}^{\mathrm{aniso}}\rangle\langle\hat{I}_{z,k}\rangle + A_{+,k}^{\mathrm{aniso}}\langle\hat{I}_{+,k}\rangle \\ &+ A_{-,k}^{\mathrm{aniso}}\langle\hat{I}_{-,k}\rangle\big)\end{aligned} \qquad \text{Eq. (2)}$$

The simulations of the OE and SE are reported in Figure 2 (a) as dashed lines. The simulations used the measured intrinsic nuclear spin-lattice relaxation times (0.45 for linear PA and 0.5 s for cyclic PA sample #2), and the previously reported electron spin relaxation time for linear PA (0.1 ms).[34,42]

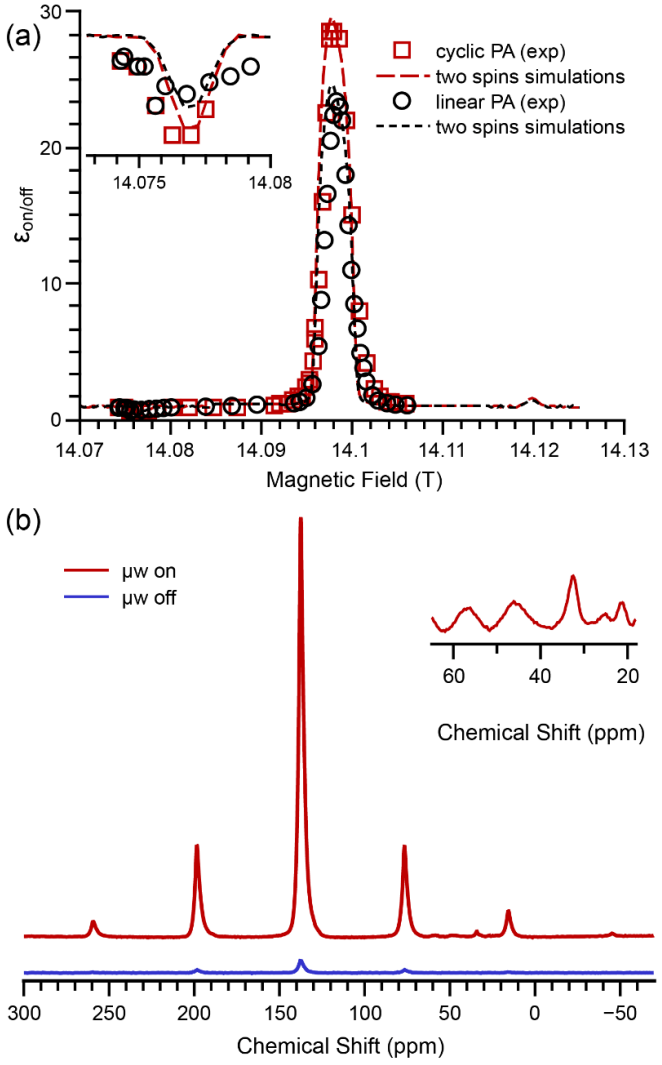

Figure 2 (a) ^{1}H MAS-DNP field profiles for linear PA (black circles) and cyclic PA (red squares, sample #2) collected at 100 K and 9.2 kHz spinning speed and the corresponding simulated enhancement using the two-spin model (dashed line, same colors) of Eq. (2). The insert is a

focused view of the Solid-Effect negative (DQ) enhancement region. (b) ^{1}H-^{13}C CP spectra of cyclic PA collected at room temperature with (red) and without (blue) w irradiation. A focused view of the cyclic PA polymer "defect" region is displayed in the insert.

The OE DNP mechanism was further explored by measuring the ^{13}C enhancement due to direct polarization (see Table 1). At 100 K, this is of the same order of magnitude as the ^{1}H enhancement. Nuclear spin diffusion between ^{13}C nuclei at natural isotopic abundance is negligible; hence, the observed large enhancement values confirm that the solitons are well delocalized over the chains.

Table 1: Measured values of the ^{1}H and ^{13}C polarization enhancements $\epsilon_{\mathrm{on/off}}$ and build-up times T_B for linear PA and cyclic PA.

	OE ^{1}H				**OE ^{13}C (direct)**	
	$\epsilon_{\mathrm{on/off}}$		T_B		max $\epsilon_{\mathrm{on/off}}$	T_B
Sample	100 K	290 K	100 K	290 K	100 K	
Linear PA	22	26	0.45 s	0.3	~20	32 s
Cyclic PA sample #1	30	45	1 s	0.5 s	~30	90 s
Cyclic PA sample #2	32	38	0.5 s	0.26 s	~48	-

Previous work on the linear *trans*-PA in the 1980s reported similar enhancements for Overhauser DNP at room temperature. However, the experiments were carried out at low field ($B_0 \leq 1.4$ T) [43] where conditions are much more favorable for DNP in a conductive material (*vide supra*). Moreover, the low magnetic fields resulted in NMR spectra of significantly lower resolution. As reported in table 2, we show the DNP enhancement in cyclic PA at 100 K exceeds that of linear PA at 14.1 T, and furthermore, the enhancement in the former is even greater at room temperature (RT). At room temperature, cyclic PA exhibits a large enhancement at the optimal OE position. This enhancement increases from ~30 at 100 K to 45 at RT for both samples tested. At RT, the buildup times are faster, yet the enhancements are higher. These increased enhancements at RT are likely due to a shortening of the correlation times favoring more efficient cross-relaxation. This observation supports, once more, the hypothesis of the existence of two populations of solitons in cyclic PA: the mobile population that generates the OE is increased at high temperature and the trapped population, that generates the SE, is increased at low temperature. Interestingly, the two cyclic PA samples displayed different nuclear polarization buildup times (0.5 s vs 1 s) which may be due to different concentration in conduction electron.

Importantly, these significant enhancements enabled for the first time the collection of ^{1}H-^{13}C Cross-Polarization (CP)[44] spectra at both temperatures with very high sensitivity. It is important to note that despite the higher enhancement at room temperature, the higher spin polarization and the better signal-to-noise performance of the NMR probe, the sensitivity remains better at the lowest temperature (see Fig. S3). The cyclic PA ^{13}C NMR spectra at 100 K, with and without w irradiation (at the maximum OE position), are reported in Figure 2 (b). The combination of high magnetic field and high signal-to-noise enabled the recording of ^{13}C signals from defect sites in the 0 to ~100 ppm chemical shift range on the neat samples. Previous low field DNP studies attempted to identify the chemical structure of defects of linear PA under oxidative condition, but the lack of resolution in that work made the assignment challenging.[43] Here we take advantage of the high resolution and very high sensitivity to address two key questions about these cyclic PA samples. Firstly, can we confirm that the chains are indeed cyclic? Secondly, what defects are observed in the neat sample?

The 1D ^{13}C NMR spectrum is dominated by the -**C**H=**C**H- signal at 136.5 ppm originating from the main chain. However, resonances at 25, 33, 46, 48, and 56 ppm are also clearly visible and correspond

to various types of "defects". Those defect signals are enhanced by the same amount as the main chain signals which indicates a close spatial proximity with the main polymers. These signals are confirmed by spectra at different MAS rates at 100 K or at room temperature (see S.I.). These signals are different than those observed in linear PA (see S.I.). The presence of signals in the 15-20 ppm range, typically associated with -CH_3, is observed for the linear PA but is absent for the cyclic PA (see Fig S4). Such methyl groups are associated with chain termination,[43] and their absence is consistent with a closed cycle PA chain topology. The signal at ~25 ppm/1.8 ppm ($^{13}C/^{1}H$ chemical shift) may correlate with the main chain but is more likely to be indicative of tetrahydrofuran solvent molecules that can remain trapped in the polymer after synthesis.

Assignment of the additional signals based on the 1D spectra is not possible or at least ambiguous. Therefore, we took advantage of the high sensitivity to carry out ^{1}H-^{13}C correlation experiments with different CP times to assess the proximity of the sites to solitons. Figure 3 reports the correlations obtained using a contact time of 40 ?s and 400 ?s. In the first case, the spin diffusion among ^{1}H nuclear spins during CP is minimal and thus no long range correlations are observed. For the longer CP time, the spin diffusion among proximal ^{1}H nuclear spins, enables probing of the chemical nature of the ^{1}H surrounding the ^{13}C sites. Based on this approach, the signals at 33 ppm (1.8-2 ppm in the ^{1}H frequency dimension) correlates with the main peak at 136.5 ppm. These carbons belong to the main chain and their chemical shift indicates they are saturated sites =CH-**C**H_2-**C**H_2-CH= as shown in Figure 3. The signals at 46 and 48 ppm correlate with the main signals at 136.5 ppm. This indicates that these carbons are close to the main chain. However, the lower cross peak intensity indicates that these sites are further away from the main chain. Finally, the peak at 56 ppm only correlates with the signal at 46 ppm but not the main chain. This site is thus even further away from the main chain as it does not correlate with it. Based on the chemical shifts, these sites could be **C**H_3-O- that are connected to the main chain via an unsaturated site -**C**H- resonating at 46 ppm. Such a site would be the result of partial oxidation on the sample's surface. It is nonetheless difficult to attribute the signal with full confidence.

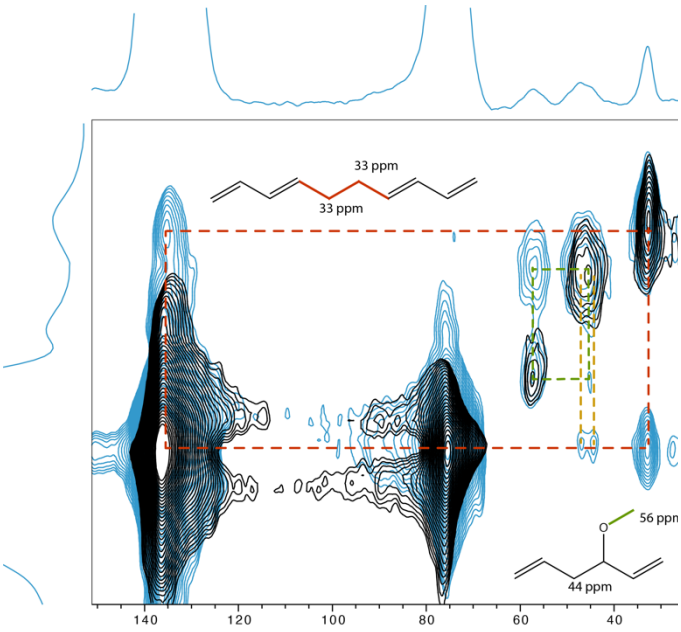

Figure 3 ^{1}H-^{13}C correlation for cyclic PA using two different cross-polarization contact times, 40 μs (black) and 400 μs (blue). Spectra were collected at 100 K and 9.2 kHz.

In summary, this study unequivocally establishes the feasibility of Dynamic Nuclear Polarization (DNP) on conductive polymers at very high magnetic fields, utilizing solitons as a nuclear hyperpolarization source. The experiments, performed on linear PA and the recently synthesized cyclic PA, revealed a remarkable enhancement which is attributed to the Overhauser effect (OE) originating from the solitons, which intriguingly persists even at room temperature where an enhancement factor of 45 was reached, a record for intrinsic defects under such magnetic field.

The combination of enhanced sensitivity and high resolution was instrumental in determining the structural composition of the defects in cyclic PA. Notably, the absence of methyl groups within the cyclic PA is unveiled, further confirming its inherent cyclic nature, and excluding the presence of detectable linear chains. This groundbreaking achievement not only advances our understanding of cyclic PA but also establishes an unforeseen pathway towards the comprehensive analysis of conductive polymers, which are pivotal

components in the landscape of molecular electronics and optoelectronics.[1]

ASSOCIATED CONTENT

Experimental details and associated content are available in the Supporting Information: unexpectedOE-SI.pdf

AUTHOR INFORMATION

Frédéric Mentink-Vigier: National High Magnetic Field Laboratory, Florida State University, 1800 E. Paul Dirac Dr, Tallahassee, FL, 32310, USA. ORCID: 0000-0002-3570-9787, Email: fmentink@magnet.fsu.edu

Zhihui Miao: Department of Chemistry, University of Florida, Center for Catalysis, PO Box 117200, Gainesville, FL 32611-7200 USA. Email: zmiao@mmm.com

Faith J. Scott: National High Magnetic Field Laboratory, Florida State University, 1800 E. Paul Dirac Dr, Tallahassee, FL, 32310, USA. ORCID: 0000-0003-3903-8842, Email: fscott@magnet.fsu.edu

Johan van Tol: National High Magnetic Field Laboratory, Florida State University, 1800 E. Paul Dirac Dr, Tallahassee, FL, 32310, USA. ORCID: 0000-0001-6972-2149, Email: fscott@magnet.fsu.edu

Clifford R. Bowers: Department of Chemistry and National High Magnetic Field Lab, University of Florida, PO Box 117200, Gainesville, FL 32611-7200 USA. ORCID: 0000-0001-6155-5163, Email: bowers@chem.ufl.edu

Adam S. Veige: Department of Chemistry, University of Florida, Center for Catalysis, PO Box 117200, Gainesville, FL 32611-7200 USA. ORCID: 0000-0002-7020-9251, Email: veige@chem.ufl.edu

ACKNOWLEDGMENTS

The National High Magnetic Field Laboratory (NHMFL) is funded by the National Science Foundation Division of Materials Research (DMR-1644779 and DMR-2128556) and the State of Florida. A portion of this work was supported by the NIH RM1-GM148766 and the European Union's Horizon 2020 Research and Innovation Programme under grant agreement no. 101008500. FJS acknowledges support from a Diversity Postdoctoral Scholar award from the Provost's Office at Florida State University. CRB acknowledges support from NSF grants CHE-2108306 and CBET-1933723. ASV acknowledges support from NSF grant CHE-2108266.

REFERENCES

(1) Nezakati, T.; Seifalian, A.; Tan, A.; Seifalian, A. M. Conductive Polymers: Opportunities and Challenges in Biomedical Applications. *Chem. Rev.* **2018**, *118* (14), 6766–6843. https://doi.org/10.1021/acs.chemrev.6b00275.

(2) Natta, G.; Mazzanti, G.; Corradini, P. Atti Accad. Naz. Lincei, Cl. *Sci. Fis. Mat. Nat., Rend* **1958**, *25* (3).

(3) Ito, T.; Shirakawa, H.; Ikeda, S. Simultaneous Polymerization and Formation of Polyacetylene Film on the Surface of Concentrated Soluble Ziegler-type Catalyst Solution. *J. Polym. Sci. Polym. Chem. Ed.* **1974**, *12* (1), 11–20. https://doi.org/10.1002/pol.1974.170120102.

(4) Shirakawa, H.; Ikeda, S. Infrared Spectra of Poly(Acetylene). *Polym. J.* **1971**, *2* (2), 231–244. https://doi.org/10.1295/polymj.2.231.

(5) Shirakawa, H.; Louis, E. J.; MacDiarmid, A. G.; Chiang, C. K.; Heeger, A. J. Synthesis of Electrically Conducting Organic Polymers: Halogen Derivatives of Polyacetylene, $(CH)_x$. *J. Chem. Soc., Chem. Commun.* **1977**, No. 16, 578. https://doi.org/10.1039/c39770000578.

(6) Chiang, C. K.; Fincher, C. R.; Park, Y. W.; Heeger, A. J.; Shirakawa, H.; Louis, E. J.; Gau, S. C.; MacDiarmid, A. G. Electrical Conductivity in Doped Polyacetylene. *Phys. Rev. Lett.* **1977**, *39* (17), 1098–1101. https://doi.org/10.1103/PhysRevLett.39.1098.

(7) Chien, J. C. W.; Karasz, F. E.; Wnek, G. E. Soliton Formation and Cis Trans Isomerization in Polyacetylene. *Nature* **1980**, *285* (5764), 390–392. https://doi.org/10.1038/285390a0.

(8) Miao, Z.; Gonsales, S. A.; Ehm, C.; Mentink-Vigier, F.; Bowers, C. R.; Sumerlin, B. S.; Veige,

A. S. Cyclic Polyacetylene. *Nat. Chem.* **2021**, *13* (8), 792–799. https://doi.org/10.1038/s41557-021-00713-2.

(9) Miao, Z.; Esper, A. M.; Nadif, S. S.; Gonsales, S. A.; Sumerlin, B. S.; Veige, A. S. Semi-Conducting Cyclic Copolymers of Acetylene and Propyne. *React. Funct, Polym.* **2021**, *169*, 105088. https://doi.org/10.1016/j.reactfunctpolym.2021.105088.

(10) Miao, Z.; Konar, D.; Sumerlin, B. S.; Veige, A. S. Soluble Polymer Precursors via Ring-Expansion Metathesis Polymerization for the Synthesis of Cyclic Polyacetylene. *Macromolecules* **2021**, *54* (17), 7840–7848. https://doi.org/10.1021/acs.macromol.1c00938.

(11) Jakhar, V. K.; Shen, Y.-H.; Hyun, S.-M.; Esper, A. M.; Ghiviriga, I.; Abboud, K. A.; Lester, D. W.; Veige, A. S. Improved Trianionic Pincer Ligand Synthesis for Cyclic Polymer Catalysts. *Organometallics* **2023**, *42* (12), 1339–1346. https://doi.org/10.1021/acs.organomet.3c00060.

(12) Kuppuswamy, S.; Peloquin, A. J.; Ghiviriga, I.; Abboud, K. A.; Veige, A. S. Synthesis and Characterization of Tungsten(VI) Alkylidene Complexes Supported by an $[OCO]^{3-}$ Trianionic Pincer Ligand: Progress towards the $[^{t}BuOCO]W{\equiv}CC(CH_3)_3$ Fragment. *Organometallics* **2010**, *29* (19), 4227–4233. https://doi.org/10.1021/om100189b.

(13) McGowan, K. P.; O'Reilly, M. E.; Ghiviriga, I.; Abboud, K. A.; Veige, A. S. Compelling Mechanistic Data and Identification of the Active Species in Tungsten-Catalyzed Alkyne Polymerizations: Conversion of a Trianionic Pincer into a New Tetraanionic Pincer-Type Ligand. *Chem. Sci.* **2013**, *4* (3), 1145–1155. https://doi.org/10.1039/C2SC21750C.

(14) Roland, C. D.; Li, H.; Abboud, K. A.; Wagener, K. B.; Veige, A. S. Cyclic Polymers from Alkynes. *Nat. Chem.* **2016**, *8* (8), 791–796. https://doi.org/10.1038/nchem.2516.

(15) Sarkar, S.; McGowan, K. P.; Kuppuswamy, S.; Ghiviriga, I.; Abboud, K. A.; Veige, A. S. An OCO^{3-} Trianionic Pincer Tungsten(VI) Alkylidyne: Rational Design of a Highly Active Alkyne Polymerization Catalyst. *J. Am. Chem. Soc.* **2012**, *134* (10), 4509–4512. https://doi.org/10.1021/ja2117975.

(16) Lilly Thankamony, A. S.; Wittmann, J. J.; Kaushik, M.; Corzilius, B. Dynamic Nuclear Polarization for Sensitivity Enhancement in Modern Solid-State NMR. *Prog. Nucl. Magn. Reson. Spectrosc.* **2017**, *102–103*, 120–195. https://doi.org/10.1016/j.pnmrs.2017.06.002.

(17) Rankin, A. G. M.; Trébosc, J.; Pourpoint, F.; Amoureux, J.-P.; Lafon, O. Recent Developments in MAS DNP-NMR of Materials. *Solid State Nucl. Magn. Reson.* **2019**, *101*, 116–143. https://doi.org/10.1016/j.ssnmr.2019.05.009.

(18) Lee, D.; Hediger, S.; De Paëpe, G. Is Solid-State NMR Enhanced by Dynamic Nuclear Polarization? *Solid State Nucl. Magn. Reson.* **2015**, *66–67*, 6–20. https://doi.org/10.1016/j.ssnmr.2015.01.003.

(19) Reif, B.; Ashbrook, S. E.; Emsley, L.; Hong, M. Solid-State NMR Spectroscopy. *Nat. Rev. Methods Primers* **2021**, *1* (1), 1–23. https://doi.org/10.1038/s43586-020-00002-1.

(20) Rossini, A. J.; Zagdoun, A.; Lelli, M.; Lesage, A.; Coperet, C.; Emsley, L. Dynamic Nuclear Polarization Surface Enhanced NMR Spectroscopy. *Acc. Chem. Res.* **2013**, *46* (9), 1942–1951. https://doi.org/10.1021/ar300322x.

(21) Maly, T.; Debelouchina, G. T.; Bajaj, V. S.; Hu, K.-N.; Joo, C.-G.; Mak-Jurkauskas, M. L.; Sirigiri, J. R.; van der Wel, P. C. A.; Herzfeld, J.; Temkin, R. J.; Griffin, R. G. Dynamic Nuclear Polarization at High Magnetic Fields. *J. Chem. Phys.* **2008**, *128* (5), 052211. https://doi.org/10.1063/1.2833582.

(22) Hope, M. A.; Rinkel, B. L. D.; Gunnarsdóttir, A. B.; Märker, K.; Menkin, S.; Paul, S.; Sergeyev, I. V.; Grey, C. P. Selective NMR Observation of the SEI–Metal Interface by Dynamic Nuclear Polarisation from Lithium Metal. *Nat. Commun.* **2020**, *11* (1), 2224. https://doi.org/10.1038/s41467-020-16114-x.

(23) Lelli, M.; Chaudhari, S. R.; Gajan, D.; Casano, G.; Rossini, A. J.; Ouari, O.; Tordo, P.; Lesage, A.; Emsley, L. Solid-State Dynamic Nuclear

Polarization at 9.4 and 18.8 T from 100 K to Room Temperature. *J. Am. Chem. Soc.* **2015**, *137* (46), 14558–14561. https://doi.org/10.1021/jacs.5b08423.
(24) Hope, M. A.; Björgvinsdóttir, S.; Halat, D. M.; Menzildjian, G.; Wang, Z.; Zhang, B.; MacManus-Driscoll, J. L.; Lesage, A.; Lelli, M.; Emsley, L.; Grey, C. P. Endogenous ^{17} O Dynamic Nuclear Polarization of Gd-Doped CeO_2 from 100 to 370 K. *J. Phys. Chem. C* **2021**, *125* (34), 18799–18809. https://doi.org/10.1021/acs.jpcc.1c04479.
(25) Hall, D. A.; Maus, D. C.; Gerfen, G. J.; Inati, S. J.; Becerra, L. R.; Dahlquist, F. W.; Griffin, R. G. Polarization-Enhanced NMR Spectroscopy of Biomolecules in Frozen Solution. *Science* **1997**, *276* (5314), 930–932. https://doi.org/10.1126/science.276.5314.930.
(26) Thurber, K. R.; Tycko, R. Theory for Cross Effect Dynamic Nuclear Polarization under Magic-Angle Spinning in Solid State Nuclear Magnetic Resonance: The Importance of Level Crossings. *J. Chem. Phys.* **2012**, *137* (8), 084508. https://doi.org/10.1063/1.4747449.
(27) Mentink-Vigier, F.; Akbey, U.; Hovav, Y.; Vega, S.; Oschkinat, H.; Feintuch, A. Fast Passage Dynamic Nuclear Polarization on Rotating Solids. *J. Magn. Reson.* **2012**, *224*, 13–21. https://doi.org/10.1016/j.jmr.2012.08.013.
(28) DeHaven, B. A.; Tokarski, J. T.; Korous, A. A.; Mentink-Vigier, F.; Makris, T. M.; Brugh, A. M.; Forbes, M. D. E.; van Tol, J.; Bowers, C. R.; Shimizu, L. S. Persistent Radicals of Self-assembled Benzophenone *Bis*-Urea Macrocycles: Characterization and Application as a Polarizing Agent for Solid-state DNP MAS Spectroscopy. *Chem. Eur. J.* **2017**, *23* (34), 8315–8319. https://doi.org/10.1002/chem.201701705.
(29) Harchol, A.; Reuveni, G.; Ri, V.; Thomas, B.; Carmieli, R.; Herber, R. H.; Kim, C.; Leskes, M. Endogenous Dynamic Nuclear Polarization for Sensitivity Enhancement in Solid-State NMR of Electrode Materials. *J. Phys. Chem. C* **2020**, *124* (13), 7082–7090. https://doi.org/10.1021/acs.jpcc.0c00858.
(30) Carnahan, S. L.; Chen, Y.; Wishart, J. F.; Lubach, J. W.; Rossini, A. J. Magic Angle Spinning Dynamic Nuclear Polarization Solid-State NMR Spectroscopy of γ-Irradiated Molecular Organic Solids. *Solid State Nucl. Magn. Reson.* **2022**, *119*, 101785. https://doi.org/10.1016/j.ssnmr.2022.101785.
(31) Shen, Y-H; Yadav, R.; Wong, A. J.; Balzer, A. H.; Epps, T. H.; Sumerlin, B. S.; Veige, A. S. Fibril Size Control, Tensile Strength, and Electrical Properties of Cyclic Polyacetylene. *React. Funct, Polym.* **2023**, *accepted.*
(32) Heeger, A. J.; Kivelson, S.; Schrieffer, J. R.; Su, W.-P. Solitons in Conducting Polymers. *Rev. Mod. Phys.* **1988**, *60* (3), 781–850. https://doi.org/10.1103/RevModPhys.60.781.
(33) Kuroda, S.; Shirakawa, H. Electron-Nuclear Double-Resonance Evidence for the Soliton Wave Function in Polyacetylene. *Phys. Rev. B* **1987**, *35* (17), 9380–9382. https://doi.org/10.1103/PhysRevB.35.9380.
(34) Clark, W. G.; Glover, K.; Mozurkewich, G.; Etemad, S.; Maxfield, M. Measurements of Soliton Trapping and Motion in Trans-Polyacetylene Using Dynamic Nuclear Polarization. *Mol. Cryst. Liq.* **1985**, *117* (1), 447–454. https://doi.org/10.1080/00268948508074663.
(35) Potje-Kamloth, K. Chapter 11: Conducting Polymer-based Schottky Barrier and Heterojunction Diodes and their Sensor Application. In *Handbook of Surfaces and Interfaces of Materials*; Nalwa, H. S., Ed.; Academic Press: Burlington, 2001; pp 445–494. https://doi.org/10.1016/B978-012513910-6/50068-2.
(36) Overhauser, A. Polarization of Nuclei in Metals. *Phys. Rev.* **1953**, *92* (2), 411–415. https://doi.org/10.1103/PhysRev.92.411.
(37) Carver, T. R.; Slichter, C. P. Experimental Verification of the Overhauser Nuclear Polarization Effect. *Phys. Rev.* **1956**, *102* (4), 975–980. https://doi.org/10.1103/PhysRev.102.975.
(38) Can, T. V.; Caporini, M. a.; Mentink-Vigier, F.; Corzilius, B.; Walish, J. J.; Rosay, M.; Maas, W. E.; Baldus, M.; Vega, S.; Swager, T. M.; Griffin, R. G. Overhauser Effects in Insulating Solids. *J. Chem. Phys.* **2014**, *141* (6), 064202. https://doi.org/10.1063/1.4891866.

(39) Wind, R. A.; Duijvestijn, M. J.; van der Lugt, C.; Manenschijn, A.; Vriend, J. Applications of Dynamic Nuclear Polarization in ^{13}C NMR in Solids. *Prog. Nucl. Magn. Reson. Spectrosc.* **1985**, *17*, 33–67. https://doi.org/10.1016/0079-6565(85)80005-4.

(40) Hovav, Y.; Feintuch, A.; Vega, S. Theoretical Aspects of Dynamic Nuclear Polarization in the Solid State - the Solid Effect. *J. Magn. Reson.* **2010**, *207* (2), 176–189. https://doi.org/10.1016/j.jmr.2010.10.016.

(41) Binet, L.; Gourier, D. Bistable Magnetic Resonance of Conduction Electrons in Solids. *J. Phys. Chem.* **1996**, *100* (44), 17630–17639. https://doi.org/10.1021/jp962094y.

(42) Völkel, G.; Dzuba, S. A.; Bartl, A.; Brunner, W.; Fröhner, J. Time-Resolved EPR on Polyacetylene. *physica status solidi (a)* **1984**, *85* (1), 257–263. https://doi.org/10.1002/pssa.2210850132.

(43) Wind, R. A.; Duijvestijn, M. J.; Vriend, J. Structural Defects in Undoped Trans-Polyacetylene, before and after Air Oxidation, Studied by DNP-Enhanced 13C NMR. *Solid State Commun.* **1985**, *56* (8), 713–716. https://doi.org/10.1016/0038-1098(85)90785-9.

(44) Pines, A.; Gibby, M. G.; Waugh, J. S. Proton-enhanced NMR of Dilute Spins in Solids. *The J. Chem. Phys.* **1973**, *59* (2), 569–590. https://doi.org/10.1063/1.1680061.